

Regular Article

# Reservoir computing reconstructs blood-oxygen-level-dependent signals: whole-brain modeling study

Artem Badarin<sup>1,a</sup>, Vladimir Klinshov<sup>2,3,b</sup>, Pavel Smelov<sup>1,c</sup>, and Andrey Andreev<sup>1,d</sup>

- Baltic Center for Neurotechnology and Artificial Intelligence, Immanuel Kant Baltic Federal University, 14 A. Nevskogo ul., Kaliningrad 236016, Russia
- <sup>2</sup> A. V. Gaponov-Grekhov Institute of Applied Physics of the Russian Academy of Sciences, 46 Ul'yanov Street, Nizhny Novgorod 603155, Russia
- <sup>3</sup> National Research University Higher School of Economics, 25/12 Bol'shaya Pecherskaya street, Nizhny Novgorod 603155, Russia

Received 1 April 2025 / Accepted 19 May 2025 / Published online 25 May 2025  $\odot$  The Author(s), under exclusive licence to EDP Sciences, Springer-Verlag GmbH Germany, part of Springer Nature 2025

Abstract Understanding and reconstructing brain dynamics from partial or noisy neuroimaging data remains a critical challenge in computational neuroscience. This study presents a novel framework combining neural mass modeling and reservoir computing (RC) to recover missing blood-oxygen-level-dependent (BOLD) signals while preserving functional connectivity patterns. We first simulate whole-brain dynamics using a Wilson–Cowan neural mass model with biologically realistic structural connectivity, optimizing parameters to match empirical functional connectivity matrices. Next, we employ RC to reconstruct individual BOLD signals using only the remaining signals as inputs. Our results demonstrate that RC achieves high-fidelity signal recovery, particularly for strongly interconnected regions. Crucially, the functional connectivity matrices derived from reconstructed signals show near-perfect agreement with the original simulated matrices, despite minor amplitude discrepancies. This work establishes RC as an effective tool for neuroimaging data reconstruction, with direct applications in both research and clinical settings where data loss or artifacts may compromise analyses.

### 1 Introduction

Currently, a rapidly developing area of scientific research is the recovery of hidden data in experimentally studied systems, which can manifest itself in such aspects as the recovering hidden features of the system to build an adequate model [1], data supplementation based on the restored features of the system [2, 3], recovering signals lost during the experiment [4, 5], recovering data that cannot be measured directly [6, 7].

One of the key areas in which the described problem is quite acute is neuroscience, where some of the experimentally recorded signals of brain activity may be missing for some reason. One of these signals is blood-oxygen-level-dependent (BOLD) one measured by functional magnetic resonance imaging (fMRI). The BOLD signal arises from neurovascular coupling, where localized neural activity triggers hemodynamic changes [8]. Multivariate BOLD signals and the derived brain functional networks serve as a robust methodological framework for the diagnosis of various neurological and psychiatric disorders [9–11]. These include, but are not limited to, major depressive disorder [12], Alzheimer's disease [13], mild cognitive impairment [14], and chronic disorders of consciousness [15]. Recent advances in computational neuroscience have further enhanced diagnostic accuracy through the integration of machine learning and deep learning techniques [16, 17].

To elucidate the underlying neural mechanisms, researchers frequently employ numerical simulations of wholebrain dynamics based on neuroimaging data [18, 19]. Such computational approaches provide valuable insights



<sup>&</sup>lt;sup>a</sup>e-mail: badarin.a.a@mail.ru

<sup>&</sup>lt;sup>b</sup>e-mail: vladimir.klinshov@gmail.com

<sup>&</sup>lt;sup>c</sup> e-mail: psmelov@kantiana.ru

<sup>&</sup>lt;sup>d</sup>e-mail: andreevandrei1993@gmail.com (corresponding author)

into the spatiotemporal organization of brain activity, facilitating a deeper understanding of both normal and pathological brain function. The whole-brain modeling is a field of neuroscience which develops and studies computational models of whole-brain neural activity. This activity depends on three major ingredients: anatomical connectivity, local neural dynamics and external input. One of the important directions in whole-brain modeling is the study of the brain resting state in which the external input is absent, and the brain is considered as an autonomous dynamical system. The central approach of the modern whole-brain modeling is to consider the brain as a dynamical network of interacting nodes. Each node represents certain brain region defined by neuroimaging-based brain parcellations, while connectivity between the nodes is derived from neuroimaging-based anatomical connectivity measurements. Thus, to obtain the model of the whole brain, it remains to define the local dynamics of the nodes and set parameters, such as the connections strength, excitability, and noise level. However, the local dynamics and the parameters can vary quite widely, which raises the question of their proper choice.

As for the local dynamics of the brain regions, it is typically described by the so-called neural mass models. These are low-dimensional dynamical systems describing the activity of neural populations in terms of averaged variables such as mean membrane potential or mean firing rate. There are many different neural mass models popular and useful in various contexts, such as Wilson–Cowan model [20], Jansen–Rit model [21], and Wong–Wang–Deco model [22]. Recently, the so-called next-generation neural mass models rapidly gain popularity [23–26]. Next-generation models were proved useful in a number of contexts including the modeling of  $\beta$  and  $\gamma$  oscillations [27], working memory [28], and whole-brain simulations [29]. Within this approach, individual brain regions or even the brain as a whole can be considered as a system of interacting populations.

As for the choice of parameters for the whole-brain model, the most reasonable approach is to fit the model so that it best reproduces some experimentally observed functional properties of the brain. In the studies devoted to the resting-state modeling, the common objective of the parameters tuning is the similarity between the simulated and empirical functional connectivity matrices [22, 30–32].

One of the most powerful paradigms for modeling and prediction of complex dynamical systems is the Reservoir computing (RC), leveraging the inherent computational capabilities of recurrent neural networks (RNNs) with fixed, randomly initialized weights [33, 34]. Unlike traditional RNNs that require costly training of recurrent connections, RC only trains a linear readout layer, making it highly efficient for time-series prediction and system identification [35]. This approach has found success in diverse applications, including chaotic system forecasting [36], macroscopic signals prediction [37] and recovering the macroscopic model and experimental signals [5]. RC's ability to approximate nonlinear dynamical systems with minimal training data makes it particularly appealing for modeling large-scale brain activity, where mechanistic simulations are often computationally prohibitive.

In this paper, we address the challenge of reconstructing missing BOLD signals by combining biologically plausible neural mass modeling with data-driven reservoir computing. We numerically simulate the dynamics of BOLD signals using neural mass models and the brain connectomes of the healthy subjects. The quality of simulation is estimated by comparing the functional connectivity matrices. We investigate the capability of recovering one of the signals using reservoir computing and applying all other signals as the input ones. We show that the functional connectivity matrices constructed from the recovered signals are perfectly coincide with the modeled ones.

# 2 Methods

### 2.1 Neural mass model

In our study, we used the whole-brain model as a network of  $N_n = 70$  nodes, each representing one brain region according to Desikan–Killiany brain parcellation scheme [38]. Each node was modeled by a Wilson–Cowan model [20]:

$$\tau_E \frac{\mathrm{d}E_i(t)}{\mathrm{d}t} = -E_i(t) + S\left(\eta + c_{EE}E_i(t) - c_{EI}I_i(t) + \sum_{j \neq i} C_{ij}E_j(t - \tau_{ij})\right) + \sigma\xi_i(t),\tag{1a}$$

$$\tau_I \frac{\mathrm{d}I_i(t)}{\mathrm{d}t} = -I_i(t) + S(c_{IE}E_i(t) - c_{II}I_i(t)) + \sigma\chi_i(t), \tag{1b}$$

where  $i, j = 1, ..., N_n$  are the brain region indices,  $E_i$  and  $I_i$  are mean firing rates of excitatory and inhibitory populations from the *i*-th region,  $\tau_E$  and  $\tau_I$  are the membrane time constants of the excitatory and inhibitory populations,  $\eta$  is the bias current to the excitatory populations,  $C_{EE}$ ,  $C_{EI}$ ,  $C_{IE}$  and  $C_{II}$  characterize the coupling between local excitatory and inhibitory populations,  $c_{ij}$  define the coupling between the *i*-th and the *j*-th regions,  $\tau_{ij}$  are the coupling delays between the *i*-th and the *j*-th regions,  $\sigma$  is the noise strength,  $\xi_i(t)$  and  $\chi_i(t)$  are the



independent standard white noise signals with zero mean and unit variance, and  $S(\cdot)$  is the sigmoid-like activation function

$$S(x) = (1 + \exp(-\lambda \beta)) \left[ (1 + \exp(\lambda (\beta - x)))^{-1} - (1 + \exp(\lambda \beta))^{-1} \right]$$
 (2)

with  $\lambda = 20$  and  $\beta = 0.3$ .

The connectivity of the network was derived from the public dataset [31] which provides structural connectivity matrices of 200 health subjects. In particular, the coupling weights  $C_{ij}$  were calculated as

$$C_{ij} = G \frac{SC_{ij}}{N_n \langle SC \rangle},\tag{3}$$

where G is the global coupling coefficient, SC is the structural connectivity matrix from the dataset, and  $\langle SC \rangle$  is the mean of its off-diagonal elements. Similarly, the delays  $\tau_{ij}$  were calculated as

$$\tau_{ij} = D \frac{PL_{ij}}{\langle PL \rangle},\tag{4}$$

where D is the coupling delay coefficient, PL is the path length matrix from the dataset, and  $\langle PL \rangle$  is the mean of its off-diagonal elements.

The whole-brain model was simulated for 300 s using the Euler integration scheme with the time step  $\delta t=1$  ms. Then the first 50 s were dropped, and the remaining 250 s were used for the parameters tuning. For this sake, the simulated activity of the regions was projected to the BOLD signals using the Balloon-Windkessel model [39]:

$$\frac{\mathrm{d}s_i}{\mathrm{d}t} = E_i - \kappa s_i - \gamma (f_i - 1),\tag{5}$$

$$\frac{\mathrm{d}f_i}{\mathrm{d}t} = s_i,\tag{6}$$

$$\tau \frac{\mathrm{d}v_i}{\mathrm{d}t} = f_i - v_i^{1/\alpha},\tag{7}$$

$$\tau \frac{dq_i}{dt} = \frac{f_i (1 - (1 - \rho)^{1/f_i})}{\rho} - \frac{v_i^{1/\alpha} q_i}{v_i},$$
(8)

where  $s_i$  is the vasodilatory signal in the *i*-th region,  $f_i$  is the blood inflow,  $v_i$  is the blood volume,  $q_i$  is the deoxyhemoglobin content,  $\kappa = 0.65 \text{ s}^{-1}$  is the signal decay rate,  $\gamma = 0.41 \text{ s}^{-1}$  is the rate of flow-dependent elimination,  $\tau = 0.98$  s is the hemodynamic transit time,  $\alpha = 0.32$  is the Grubb's exponent, and  $\rho = 0.34$  is the resting oxygen extraction fraction. The BOLD signal from the i-th region is calculated as

$$y_i = k_1(1 - q_i) + k_2(1 - q_i/v_i) + k_3(1 - v_i),$$
(9)

where  $k_1 = 7\rho$ ,  $k_2 = 2$ ,  $k_3 = 2\rho - 0.2$ .

The simulated BOLD signals of the regions were used to construct the simulated functional connectivity matrix SFC, which was compared with the empirical functional connectivity matrix EFC in order to tune the model parameters. The set of tunable parameters was  $\theta = (D, G, \eta, \sigma, c_{EE}, c_{EI}, c_{IE}, c_{II}, \tau_{E}, \tau_{I}) \in \mathbb{R}^{10}$ . We used genetic algorithms to optimize the model parameters varying them in the ranges indicated in Table 1. As the objective function to minimize, we used various types of distance measures between the simulated and empirical connectivity matrices:

- Correlation distance defined as  $d_C = 1 c$ , where c is the Pearson correlation coefficient between the vectorized 1. upper triangles of SFC and EFC.
- Euclidean distance  $d_E$  between the vectorized upper triangles of SFC and EFC. Geodesic distance defined as  $d_G = \left| \log \left( SFC^{-1/2}EFC \ SFC^{-1/2} \right) \right|_F$ , where log denotes the matrix logarithm, 3.  $A^{-1/2}$  is the inverse square root of matrix A, and  $||_F$  is the Frobenius norm [40].

During the optimization procedure, we ran tens of thousands of simulations for each of the patients which allowed to analyze the statistics of the three distance measures which is illustrated in Fig. 1. We found that the two measures are strongly correlated for all the patients: the Pearson correlation coefficient and the geodesic distance



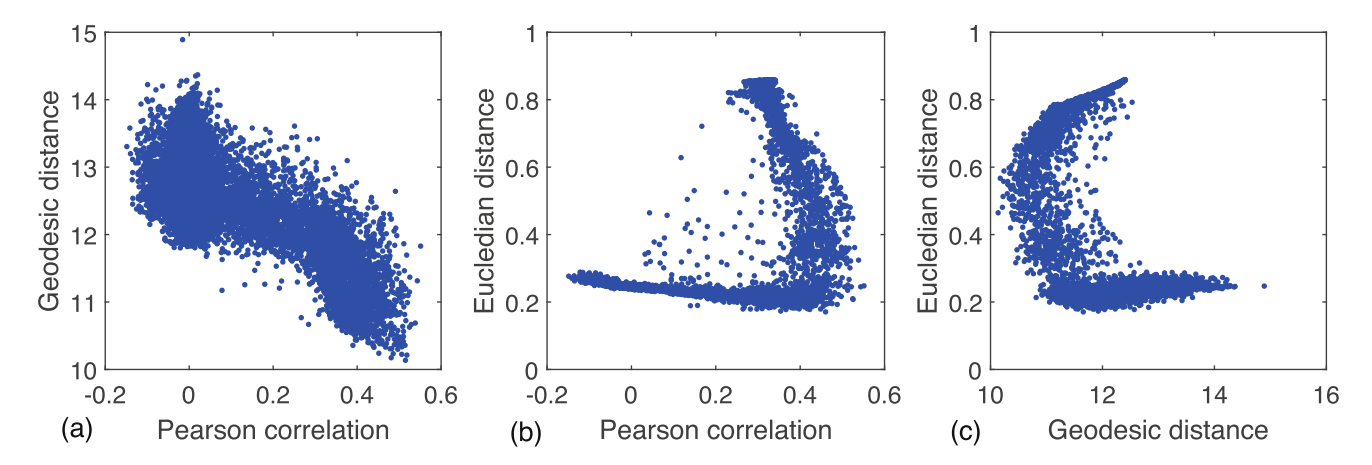


Fig. 1 The correlations between the three different measures of the similarity between the SFC and EFC matrices

**Table 1** The parameters for optimization in a model

| Parameter | Meaning                                 | Minimal value | Maximal value |
|-----------|-----------------------------------------|---------------|---------------|
| G         | Global coupling coefficient             | 0.1           | 0.5           |
| D         | Global delay coefficient                | 0             | 10            |
| $\eta$    | Bias current                            | 0.0           | 0.2           |
| $\sigma$  | Noise strength                          | 0.0           | 0.1           |
| $C_{EE}$  | Local excitatory-to-excitatory coupling | 0.5           | 2             |
| $C_{EI}$  | Local excitatory-to-inhibitory coupling | 0.5           | 2             |
| $C_{IE}$  | Local inhibitory-to-excitatory coupling | 0             | 1             |
| $C_{II}$  | Local inhibitory-to-inhibitory coupling | 0             | 1             |
| $	au_E$   | Excitatory membrane time                | 10            | 30            |
| $	au_I$   | Inhibitory membrane time                | 10            | 30            |

(Fig. 1a). At the same time, the Euclidean distance turned to be weakly correlated with the former two measures (Fig. 1b, c). These observations lead to the following solution: we used the geodesic distance as the function for optimization which also guaranteed high values of the Pearson correlation.

### 2.2 Reservoir computing

To recover the BOLD signals obtained from the network of the neural mass models, use a subclass of the recurrent neural network–reservoir computing. Figure 2 illustrates a schematic representation of the dynamics of the whole-brain model and the process of reconstruction the BOLD signals using reservoir computing. It consists of three layers: input, hidden (reservoir) and output.

The input layer consists of  $N_n-1$  input signals  $\mathbf{B}_i$  at *i*-th time moment. They are applied to the hidden layer via the input-to-hidden coupling matrix  $\mathbf{W}_{\mathrm{IH}}$  of size  $(N_n-1)\times N$ , where N in the size of the reservoir.  $\mathbf{W}_{\mathrm{IH}}$  matrix is generated randomly and characterized by the hyperparameter  $\delta_{\mathrm{IH}}$  defining the density of the connections from the input neurons to the hidden ones. The strength of the existing couplings are equal to 1, so  $\mathbf{W}_{\mathrm{IH}}$  consists of only  $\{1\}$  and  $\{0\}$  values.

The hidden neurons are described by the following equation:

$$\mathbf{h}_{i} = (1 - l)\mathbf{h}_{i-1} + l \tanh(\mathbf{W}_{\mathrm{IH}}\mathbf{B}_{i} + \mathbf{W}_{\mathrm{HH}}\mathbf{h}_{i-1}), \tag{10}$$

where l is the hyperparameter describing the leaking rate,  $\mathbf{W}_{\mathrm{HH}}$  is the hidden-to-hidden sparse matrix with size  $N \times N$  generated randomly with hyperparameters R and  $\delta_{\mathrm{HH}}$  which are the spectral radius and the density of the connections respectively.

The output layer consists of one linear neuron needed to generate the recovering signals and described as

$$o_i = \mathbf{W}_{\mathrm{HO}} \mathbf{h}_i,$$
 (11)



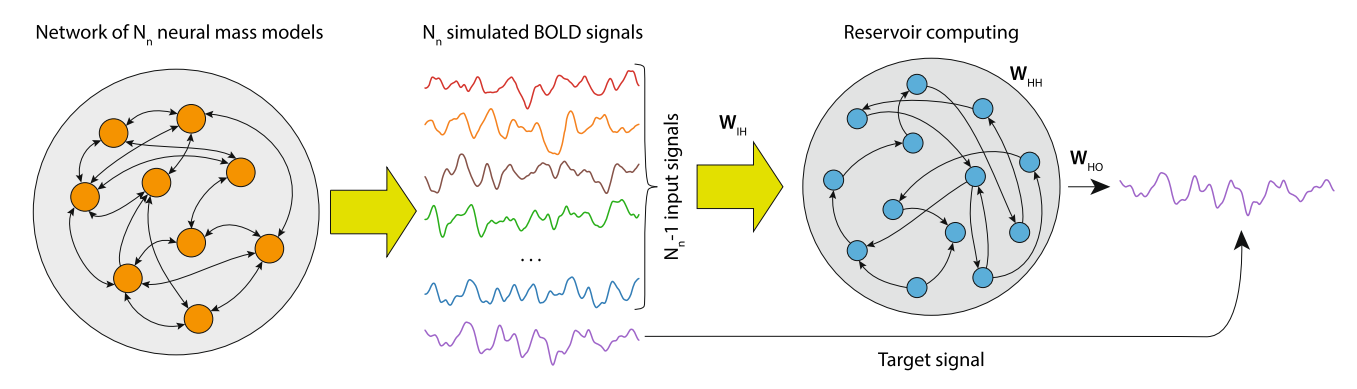


Fig. 2 A schematic representation of the dynamics of the whole-brain model and the process of reconstruction the BOLD signals using reservoir computing

where  $\mathbf{W}_{\mathrm{HO}}$  is the hidden-to-output matrix defines in the training process by minimizing the  $L_2$ -error between the target X and predicted o signals:

$$\sum_{i=1}^{T_{\text{train}}} ||o_i - y_i||^2 + b||\mathbf{W}_{\text{HO}}||^2, \tag{12}$$

where y is the target signal,  $T_{\text{train}}$  is the duration of the training process,  $b = 10^{-3}$  is the regularization parameter. After the training process is complete, we test the RC described by Eqs. (10,11), where the  $\mathbf{W}_{\mathrm{IH}}$  and  $\mathbf{W}_{\mathrm{HH}}$ matrices are the same as in the training mode, and the matrix  $\mathbf{W}_{HO}$  of the output layer is determined in the training phase by minimizing the  $L_2$ -error (12). Then, we calculate  $r^2$ -score between the predicted and the target signals to estimate the quality of prediction:

$$r^{2} = 1 - \frac{\sum_{i=1}^{T_{\text{test}}} (y_{i} - o_{i})^{2}}{\sum_{i=1}^{T_{\text{test}}} (y_{i} - \bar{y})^{2}},$$
(13)

where  $\bar{y} = \frac{1}{T_{\text{test}}} \sum_{i=1}^{T_{\text{test}}} y_i$  is the mean value of y, and  $T_{\text{test}}$  is the duration of the testing process. We optimize the hyperparameters  $R, \delta_{\text{IH}}, \delta_{\text{HH}}$ , and l by employing an optimization algorithm over the intervals [0.1, 1], [0.05, 0.5], [0.05, 0.5], and [0.1, 1.0], respectively. For each channel restoration, the optimization was conducted independently over 500 iterations, with each iteration corresponding to a distinct parameter combination; the configuration yielding the highest  $r^2$  was selected.

# 3 Results

First, we fit the parameters of neural mass model for each of five subject in order to achieve good coincidence between the connectivity matrices obtained by calculating Pearson correlation coefficient C for real and simulated BOLD signals. Figure 3a, b illustrates an example of the real and simulated connectivity matrices. As one can see, in real data there are the areas which are not correlated to any other, and the ones which are in a good correlation with the others. The simulated signals show the same pattern: one can see that the same brain areas show no correlation with others, while other signals do.

Then, for each subject we solve the task of recovering each simulated signal using all others. For that, we train the RC to recover each signal by applying all other signals as the input ones. As a result, we obtain 350 recovered signals: 70 per each subject. Figure 4a illustrates an example of the recovered signal compared to the original one. As one can see, the RC perfectly predicts all the time moments of the oscillations. The only small error occurs with the amplitude of the oscillations: RC makes it smoother.

We investigate whether there is a dependence between the original connectivity strength of the signal and the recovering accuracy. Figure 4b illustrates the dependence of  $r^2$ -score between the predicted and the target signals on the maximal connectivity strength c between the predicting and other model signals. Each cross here corresponds to each predicting signal of one of five subjects. As one can see on the right histogram, most part of the signals characterized by high accuracy  $(r^2 > 0.5)$  while the maximal connectivity strength of the most par of the signals is low (c < 0.5 on the top histogram). All signals with maximal connectivity strength more than 0.5



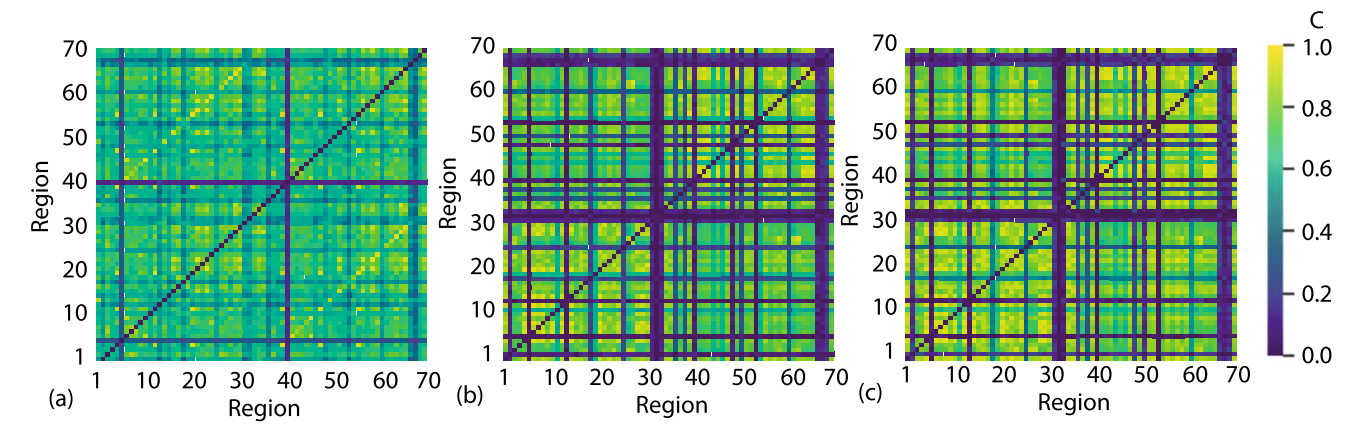
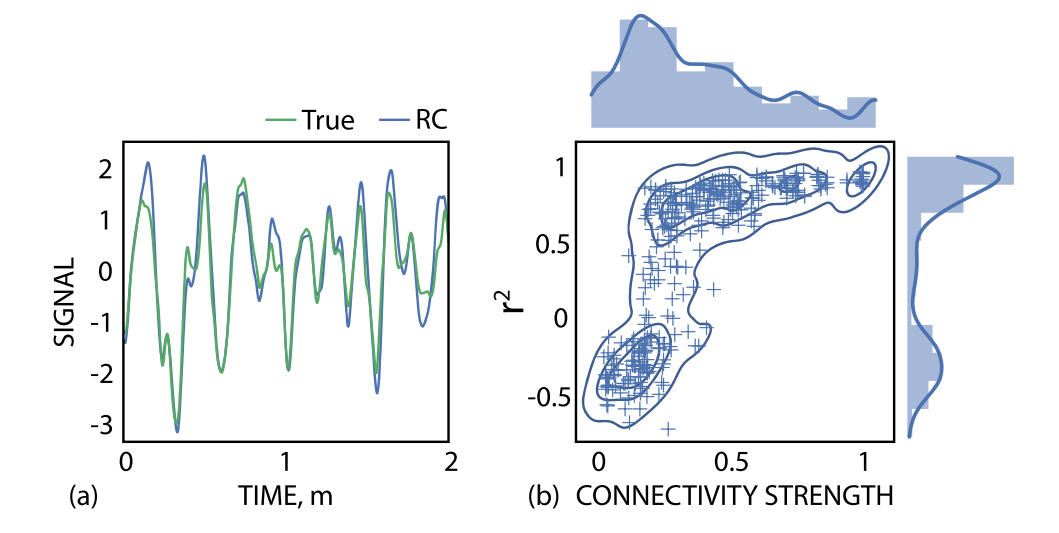


Fig. 3 The connectivity matrices between the brain regions obtained using a real BOLD signals, b simulated signals, and c recovered simulated signals

Fig. 4 a Example of RC's prediction and b the dependence of  $r^2$ -score between the predicted and the target signals on the maximal connectivity strength between the predicting and other model signals. Each cross corresponds to each predicting signal of one of five subjects



are recovered with high accuracy. Small part of the signals with c < 0.15 cannot be recovered with good accuracy  $(r^2 < 0)$ . The rest part of the signals with 0.15 < c < 0.5 can be recovered with any accuracy  $-0.8 > r^2 \le 1.0$ . We can suppose that the accuracy for that group depends not only on the maximal connectivity strength but also from the mean one: the more signals are correlated to the recovered one, the higher the mean connectivity strength and the accuracy.

As a final step, we compare the connectivity matrices obtained by simulated and recovered signals. To obtain the second one, we use only the RC's signals, without using any of the original ones. As one can see on Fig. 3c, the recovered matrix perfectly replicates the simulated one. The regions which are not connected to any other in the simulated network are similarly have no functional connectivity in the recovered data. The others have the connections with almost the same strength c as in the simulated network.

Therefore, we can conclude that despite the incapability of RC to correctly recover the signals which are weakly connected to the other ones, their macro-characteristic as the functional connectivity strength is reproduces with very high accuracy. The signals with strong connectivity can by recovered with high accuracy of both  $r^2$  and c.

### 4 Conclusions

In this study, we investigated the recovery of missing BOLD signals in whole-brain modeling using a combination of neural mass models and reservoir computing (RC). Our approach demonstrated that RC can effectively reconstruct BOLD signals from a subset of available data while preserving key functional connectivity patterns.



By tuning the parameters of the Wilson–Cowan neural mass model, we achieved a strong correspondence between simulated and empirical functional connectivity matrices. This confirms the model's ability to replicate realistic brain dynamics under resting-state conditions.

RC successfully recovered missing BOLD signals with high accuracy, particularly for signals exhibiting strong functional connectivity with other regions. The prediction quality, measured by the  $r^2$ -score, was highest for signals with maximal connectivity strength, while weakly connected signals proved more challenging to reconstruct.

Despite minor discrepancies in signal amplitude, the functional connectivity matrices derived from recovered signals closely matched those obtained from the original simulated data. This indicates that RC can reliably capture macroscopic network properties even when individual signal reconstruction is imperfect.

Our results highlight the potential of reservoir computing as a powerful tool for recovering missing or corrupted neuroimaging data, with applications in both computational neuroscience and clinical settings. Future research could explore the integration of more advanced neural mass models, the impact of noise on reconstruction accuracy, and the extension of this framework to task-based fMRI data

Acknowledgements This work is supported by the Russian Science Foundation (project 24-71-10072).

Data Availability No data associated in the manuscript.

## References

- M. Kanehisa, Y. Sato, M. Kawashima, Kegg mapping tools for uncovering hidden features in biological data. Protein Sci. 31(1), 47–53 (2022)
- Z. Zhang, T. Ji, M. Xiao, W. Wang, G. Yu, T. Lin, Y. Jiang, X. Zhou, Z. Lin, Cross-patient automatic epileptic seizure detection using patient-adversarial neural networks with spatio-temporal eeg augmentation. Biomed. Signal Process. Control 89, 105664 (2024)
- 3. M. Svantesson, H. Olausson, A. Eklund, M. Thordstein, Virtual eeg-electrodes: convolutional neural networks as a method for upsampling or restoring channels. J. Neurosci. Methods 355, 109126 (2021)
- S. Mahmud, M.E. Chowdhury, S. Kiranyaz, N. Al Emadi, A.M. Tahir, M.S. Hossain, A. Khandakar, S. Al-Maadeed, Restoration of motion-corrupted eeg signals using attention-guided operational cyclegan. Eng. Appl. Artif. Intell. 128, 107514 (2024)
- 5. A. Badarin, A. Andreev, V. Klinshov, V. Antipov, A.E. Hramov, Hidden data recovery using reservoir computing: adaptive network model and experimental brain signals. Chaos Interdiscip. J. Nonlinear Sci. 34(10) (2024)
- 6. D. Kim, A. Tran, H.J. Kim, Y. Lin, J.Y.H. Yang, P. Yang, Gene regulatory network reconstruction: harnessing the power of single-cell multi-omic data. NPJ Syst. Biol. Appl. 9(1), 51 (2023)
- H.J. Waarde, P. Tesi, M.K. Camlibel, Topology reconstruction of dynamical networks via constrained Lyapunov equations. IEEE Trans. Autom. Control 64(10), 4300–4306 (2019)
- 8. N.K. Logothetis, J. Pauls, M. Augath, T. Trinath, A. Oeltermann, Neurophysiological investigation of the basis of the fmri signal. Nature 412(6843), 150–157 (2001)
- 9. V.S. Khorev, S.A. Kurkin, G. Zlateva, R. Paunova, S. Kandilarova, M. Maes, D. Stoyanov, A.E. Hramov, Disruptions in segregation mechanisms in fmri-based brain functional network predict the major depressive disorder condition. Chaos Solitons Fract. 188, 115566 (2024)
- 10. A.E. Hramov, N.S. Frolov, V.A. Maksimenko, S.A. Kurkin, V.B. Kazantsev, A.N. Pisarchik, Functional networks of the brain: from connectivity restoration to dynamic integration. Phys. Usp. **64**(6), 584 (2021)
- 11. M.H. Lee, C.D. Smyser, J.S. Shimony, Resting-state fmri: a review of methods and clinical applications. Am. J. Neuroradiol. **34**(10), 1866–1872 (2013)
- 12. S.A. Kurkin, N.M. Smirnov, R. Paunova, S. Kandilarova, D. Stoyanov, L. Mayorova, A.E. Hramov, Beyond pairwise interactions: higher-order Q-analysis of fMRI-based brain functional networks in patients with major depressive disorder. IEEE Access 12, 197168–197186 (2024)
- 13. S. Zhang, H. Zhao, W. Wang, Z. Wang, X. Luo, A. Hramov, J. Kurths, Edge-centric effective connection network based on muti-modal mri for the diagnosis of Alzheimer's disease. Neurocomputing 552, 126512 (2023)
- W. Wang, S. Zhang, Z. Wang, X. Luo, P. Luan, A. Hramov, J. Kurths, C. He, J. Li, Diagnosis of early mild cognitive impairment based on associated high-order functional connection network generated by multimodal mri. IEEE Trans. Cogn. Dev. Syst. 16(2), 618–627 (2023)
- 15. V. Khorev, S. Kurkin, E. Pitsik, M. Radutnaya, E. Bondar, L. Mayorova, A. Hramov, A synergistic approach for identifying disrupted functional brain subnetworks in patients with chronic disorders of consciousness due to anoxic brain damage. Eur. Phys. J. Spec. Top. (2025). https://doi.org/10.1140/epjs/s11734-024-01454-2
- O.E. Karpov, E.N. Pitsik, S.A. Kurkin, V.A. Maksimenko, A.V. Gusev, N.N. Shusharina, A.E. Hramov, Analysis of publication activity and research trends in the field of ai medical applications: network approach. Int. J. Environ. Res. Public Health 20(7), 5335 (2023)



- 17. E.N. Pitsik, V.A. Maximenko, S.A. Kurkin, A.P. Sergeev, D. Stoyanov, R. Paunova, S. Kandilarova, D. Simeonova, A.E. Hramov, The topology of fmri-based networks defines the performance of a graph neural network for the classification of patients with major depressive disorder. Chaos Solitons Fract. 167, 113041 (2023)
- 18. G. Deco, V.K. Jirsa, P.A. Robinson, M. Breakspear, K. Friston, The dynamic brain: from spiking neurons to neural masses and cortical fields. PLoS Comput. Biol. 4(8), 1000092 (2008)
- 19. M. Breakspear, Dynamic models of large-scale brain activity. Nat. Neurosci. 20(3), 340-352 (2017)
- 20. H.R. Wilson, J.D. Cowan, Excitatory and inhibitory interactions in localized populations of model neurons. Biophys. J. 12(1), 1–24 (1972)
- 21. B.H. Jansen, V.G. Rit, Electroencephalogram and visual evoked potential generation in a mathematical model of coupled cortical columns. Biol. Cybern. **73**(4), 357–366 (1995)
- 22. G. Deco, A. Ponce-Alvarez, D. Mantini, G.L. Romani, P. Hagmann, M. Corbetta, Resting-state functional connectivity emerges from structurally and dynamically shaped slow linear fluctuations. J. Neurosci. 33(27), 11239–11252 (2013)
- 23. E. Montbrió, D. Pazó, A. Roxin, Macroscopic description for networks of spiking neurons. Phys. Rev. X 5(2), 021028 (2015)
- 24. Á. Byrne, D. Avitabile, S. Coombes, Next-generation neural field model: the evolution of synchrony within patterns and waves. Phys. Rev. E 99(1), 012313 (2019)
- 25. V.V. Klinshov, S.Y. Kirillov, Shot noise in next-generation neural mass models for finite-size networks. Phys. Rev. E 106(6), 062302 (2022)
- V. Klinshov, P. Smelov, S.Y. Kirillov, Constructive role of shot noise in the collective dynamics of neural networks. Chaos Interdiscip. J. Nonlinear Sci. 33(6) (2023)
- 27. A. Byrne, M.J. Brookes, S. Coombes, A mean field model for movement induced changes in the beta rhythm. J. Comput. Neurosci. 43, 143–158 (2017)
- 28. H. Taher, A. Torcini, S. Olmi, Exact neural mass model for synaptic-based working memory. PLoS Comput. Biol. **16**(12), 1008533 (2020)
- M. Gerster, H. Taher, A. Škoch, J. Hlinka, M. Guye, F. Bartolomei, V. Jirsa, A. Zakharova, S. Olmi, Patient-specific network connectivity combined with a next generation neural mass model to test clinical hypothesis of seizure propagation. Front. Syst. Neurosci. 15, 675272 (2021)
- 30. C.J. Honey, O. Sporns, L. Cammoun, X. Gigandet, J.-P. Thiran, R. Meuli, P. Hagmann, Predicting human resting-state functional connectivity from structural connectivity. Proc. Natl. Acad. Sci. 106(6), 2035–2040 (2009)
- 31. J.W. Domhof, K. Jung, S.B. Eickhoff, O.V. Popovych, Parcellation-induced variation of empirical and simulated brain connectomes at group and subject levels. Netw. Neurosci. 5(3), 798–830 (2021)
- 32. M. Hashemi, A. Ziaeemehr, M.M. Woodman, J. Fousek, S. Petkoski, V.K. Jirsa, Simulation-based inference on virtual brain models of disorders. Mach. Learn. Sci. Technol. 5(3), 035019 (2024)
- 33. H. Jaeger, The "echo state" approach to analysing and training recurrent neural networks-with an erratum note, vol. 148(34). German National Research Center for Information Technology Gmd Technical Report, Bonn, Germany (2001), p. 13
- 34. A.E. Hramov, N. Kulagin, A.N. Pisarchik, A.V. Andreev, Strong and weak prediction of stochastic dynamics using reservoir computing. Chaos Interdiscip. J. Nonlinear Sci. 35(3) (2025)
- M. Lukoševičius, H. Jaeger, Reservoir computing approaches to recurrent neural network training. Comput. Sci. Rev. 3(3), 127–149 (2009)
- 36. J. Pathak, B. Hunt, M. Girvan, Z. Lu, E. Ott, Model-free prediction of large spatiotemporally chaotic systems from data: a reservoir computing approach. Phys. Rev. Lett. 120(2), 024102 (2018)
- 37. A.V. Andreev, A.A. Badarin, V.A. Maximenko, A.E. Hramov, Forecasting macroscopic dynamics in adaptive Kuramoto network using reservoir computing. Chaos Interdiscipl. J. Nonlinear Sci. 32(10) (2022)
- 38. R.S. Desikan, F. Ségonne, B. Fischl, B.T. Quinn, B.C. Dickerson, D. Blacker, R.L. Buckner, A.M. Dale, R.P. Maguire, B.T. Hyman et al., An automated labeling system for subdividing the human cerebral cortex on mri scans into gyral based regions of interest. Neuroimage 31(3), 968–980 (2006)
- 39. K.J. Friston, L. Harrison, W. Penny, Dynamic causal modelling. Neuroimage 19(4), 1273–1302 (2003)
- M. Venkatesh, J. Jaja, L. Pessoa, Comparing functional connectivity matrices: a geometry-aware approach applied to participant identification. Neuroimage 207, 116398 (2020)

Springer Nature or its licensor (e.g. a society or other partner) holds exclusive rights to this article under a publishing agreement with the author(s) or other rightsholder(s); author self-archiving of the accepted manuscript version of this article is solely governed by the terms of such publishing agreement and applicable law.

